Picosecond ultrasonic study of surface acoustic waves on periodically patterned layered nanostructures

Michael Colletta,[a] Wanjiru Gachuhi,[a] Samuel A. Gartenstein,[a] Molly M. James,[a] Erik A. Szwed,[a] Brian C. Daly,[a†] Weili Cui,[b] George A. Antonelli,[c]

a: Vassar College, 124 Raymond Ave, Poughkeepsie, NY, USA 12604

b: SUNY Maritime College, Throggs Neck, NY, USA 10465

c: Antonelli Research and Technology, 3227 SE Lambert St, Portland, OR,USA 97202

†: corresponding author's email: brdaly@vassar.edu

Abstract:

We have used the ultrafast pump-probe technique known as picosecond ultrasonics to generate and detect surface acoustic waves on a structure consisting of nanoscale Al lines on SiO_2 on Si. We report results from ten samples with varying pitch (1000 nm to 140 nm) and SiO_2 film thickness (112 nm or 60 nm), and compare our results to an isotropic elastic calculation and a coarse-grained molecular dynamics simulation. In all cases we are able to detect and identify a Rayleigh-like surface acoustic wave with wavelength equal to the pitch of the lines and frequency in the range of 5 GHz – 24 GHz. In some samples, we are able to detect additional, higher frequency surface acoustic waves or independent modes of the Al lines with frequencies close to 50 GHz. We also describe the effects of probe beam polarization on the measurement's sensitivity to the different surface modes.

Keywords: ultrafast optics; picosecond ultrasonics; laser ultrasonics; surface acoustic waves

Introduction

The highest frequency surface acoustic waves (SAWs) have to date been generated and detected by ultrafast optical pump-probe techniques.[1,2,3,4] The most common method is to use lithography to fabricate a nanoscale pattern of metallic lines on a substrate and excite those lines by means of an ultrafast laser pulse. The rapid thermal expansion of the lines launches a SAW (often called a pseudo-SAW or leaky SAW since the presence of the pattern on the surface causes radiation of acoustic energy into the bulk) with wavelength equal to the pitch of the lines that propagates perpendicular to the lines. SAWs up to 50 GHz have been generated and detected in this manner.[5] In recent work conducted by two authors of the present article we measured SAWs or related surface vibrations in a complicated structure consisting of TiN wires of nanometer scale cross-section grown on a multilayered stack of porous and non-porous oxides on an Si wafer. [6] These unique samples yielded pitch-dependent frequencies that in some cases compared favorably with Rayleigh-like or Sezawa-like surface waves,[7,8] but in other cases corresponded to

modes that radiated significant acoustic energy into the substrate. In this work we have chosen to study a simpler set of samples consisting of Al lines on thin SiO_2 on Si and we detect multiple SAWs which can be identified by comparison with coarse-grained molecular dynamics simulations. The number of modes detected was found to depend on the pitch of the patterned Al as well as on the wavelength and polarization of the probe light. We detected Rayleigh-like SAWs and Sezawa-like SAWs with wavelength equal to the pitch of the Al lines as well as SAWs with wavelength equal to one-half or one-third of the pitch.

Experiment

The ultrafast optical pump-probe experiment known as picosecond laser ultrasonics (PLU) has been described extensively in the literature.[9,10] We performed this experiment with a Ti:Sapphire oscillator operating at a 76 MHz repetition rate with pump wavelength of 800 nm and probe wavelengths of 800 nm or 400 nm. The 400 nm probe experiments were achieved by second harmonic generation in a BiBO crystal. The 10 patterned samples that we studied are illustrated schematically in Fig. 1. The samples were fabricated at the Cornell NanoScale Facility by the following process: thermal oxidation to produce the amorphous SiO_2 layer of thickness d = 60 or 112 nm, thermal evaporation of 25 nm of Al, and E-beam lithography and dry etching to create the nanometer scale Al pattern. The lines were etched perpendicular to the [110] direction in the Si substrate, they varied in pitch p ranging from 140 nm up to 1000 nm, and they were all etched near 50% (ranging from 40-60%) duty cycle. The patterned samples were placed into the optical setup, where pump and probe beams were both focused onto the same 20 μm diameter spot, so that anywhere from 20 to 140 periods of the pattern were strongly illuminated. For the data reported here, the pump and probe beams were held normally incident. Measurements were also made with 45 degree incident probe light but only minor differences from the normal case were found. The ultrafast pump pulses were absorbed by the Al lines, and the resulting rapid thermal expansion launched ultrasonic waves both downward into the SiO_2 film and Si substrate, and laterally as SAWs in the direction perpendicular to the line pattern. The various ultrasonic waves can be detected by the time-delayed probe pulses due to transient changes in the reflectivity ΔR that they cause. The sources of these transient changes include the dependence of the optical constants of the Al on strain as well as the changes in reflectivity of the optical grating produced by the nanostructure as it responds to the acoustic oscillations. In this work, we focus on the signals caused by laterally propagating ultrasound and not the signals caused by acoustic waves traveling normal to the sample surface.

Fig. 2a shows an example of the ΔR signal with 800 nm probe as a function of probe delay time for two of the samples (p/d = 400 nm/112 nm and 200 nm/112 nm). The exponentially decaying thermal background and the initial jump at t = 0 have been subtracted off so that the dominant oscillations are easier to observe. Fig. 2b shows the Fourier transform for these two data sets. For both samples, the data are dominated by oscillations at two frequencies. As is expected, the

Figure 1

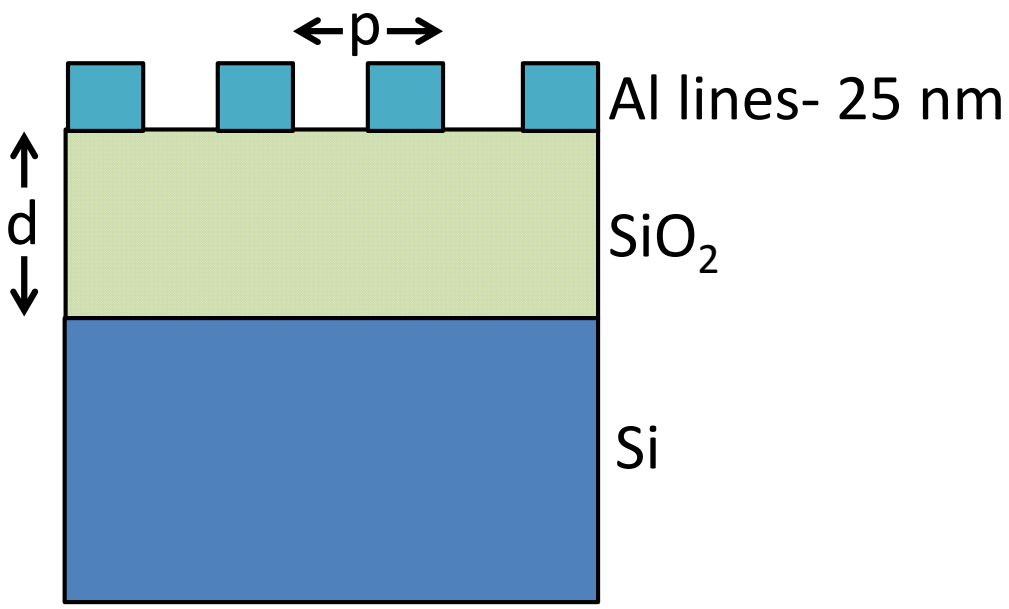

Figure 1: Schematic diagram of the samples. Film thickness *d* was either 60 nm or 112 nm as measured by picosecond ultrasonics. Al lines pitch *p* varied from 1000 nm down to 140 nm. The duty cycle was close to 50% (+/- 10%) in all cases as measured by SEM imaging.

Figure 2

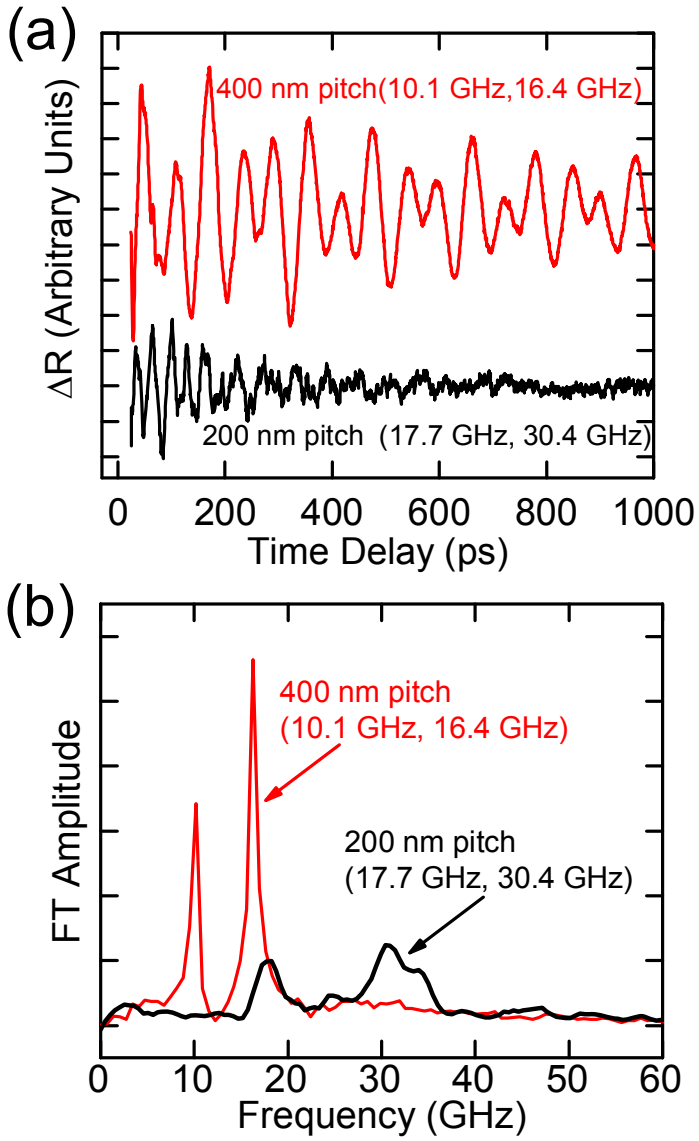

Figure 2: (a) ΔR for two samples with d =112 nm and p = 400 nm and 200 nm. (b) Fourier transform amplitude of the signals in (a).

smaller pitch sample produces higher frequency oscillations. The frequencies of the observed oscillations are strongly dependent on the pitch of the samples, and so it is evident that they must represent SAWs, independent bar modes, or a wave propagating very near to the surface of the sample. Other data sets show as few as one or as many as seven detected surface modes, and in the following sections we identify the nature of many of these modes. It is also evident from Fig. 2a that the excitations are shorter lived in the 200 nm sample as compared with the 400 nm sample. The presence of a periodic structure on a surface adds stress which in turn causes radiation of surface acoustic wave energy into the bulk - a process that was first described by Brekovskikh.[11] This is the dominant damping mechanism for SAWs on periodically patterned surfaces in the GHz range, and the damping depends on the fourth power of the SAW frequency.[4,12]

Lowest order Rayleigh-like modes

The lowest frequencies measured for all ten samples compare favorably with the expected frequency for a Rayleigh-like wave in Si in the [110] direction that is loaded by a thin oxide layer. Table I lists the frequencies of the lowest frequency oscillations detected for the 10 samples. In the only case where we measured two films with the same pitch but differing oxide thickness (p/d = 200nm/60nm and 200nm/112nm) we clearly see that the effect of the thicker oxide is to lower the frequency of the detected wave. This is expected for this situation where the SiO_2 film loads the Si substrate due to its lower density and sound velocity. Fig. 3 contains a plot of the phase velocities for the 10 measured Rayleigh-like SAWs alongside an analytical calculation of the phase velocities for an isotropic model of an SiO_2 loaded Si substrate.[8] The x-axis of the graph is the dimensionless quantity kd where k is the wavenumber of the SAW. Note that the calculation of the first Rayleigh-like mode has the Rayleigh velocity of Si for very small kd, but has the Rayleigh velocity of SiO_2 for very large kd. The data are in good agreement with the predicted velocities (deviating by between 0.7% and 8%) which is reasonable given that the experimental uncertainty in the measurement of the frequencies is 5%. The plot also shows that for a case such as this one, in which the thin film loads, rather than stiffens, the surface of the substrate, additional modes (labeled RL-2 and RL-3 in Fig. 3) appear as kd is increased. The RL-2 mode is also called a Sezawa wave.

To further confirm the nature of the SAWs that we detected, we have performed 2D coarse-grained molecular dynamics (CGMD) simulations on cross-sectional models of the nanostructures. The simulations essentially collect multiple atoms together to form larger super-atoms in order to solve the elastic motion of the cross section of the structures in question. The simulation, which has been described in detail previously,[6,13] models the materials as isotropic elastic solids with given density and transverse and longitudinal sound velocities. We simulate a 2D cross-section of one period of the structure, and implement periodic boundary conditions in the lateral directions. We also place an absorbing boundary condition at the bottom of the structure so that any simulated modes traveling into the substrate will not be reflected back to the

Figure 3

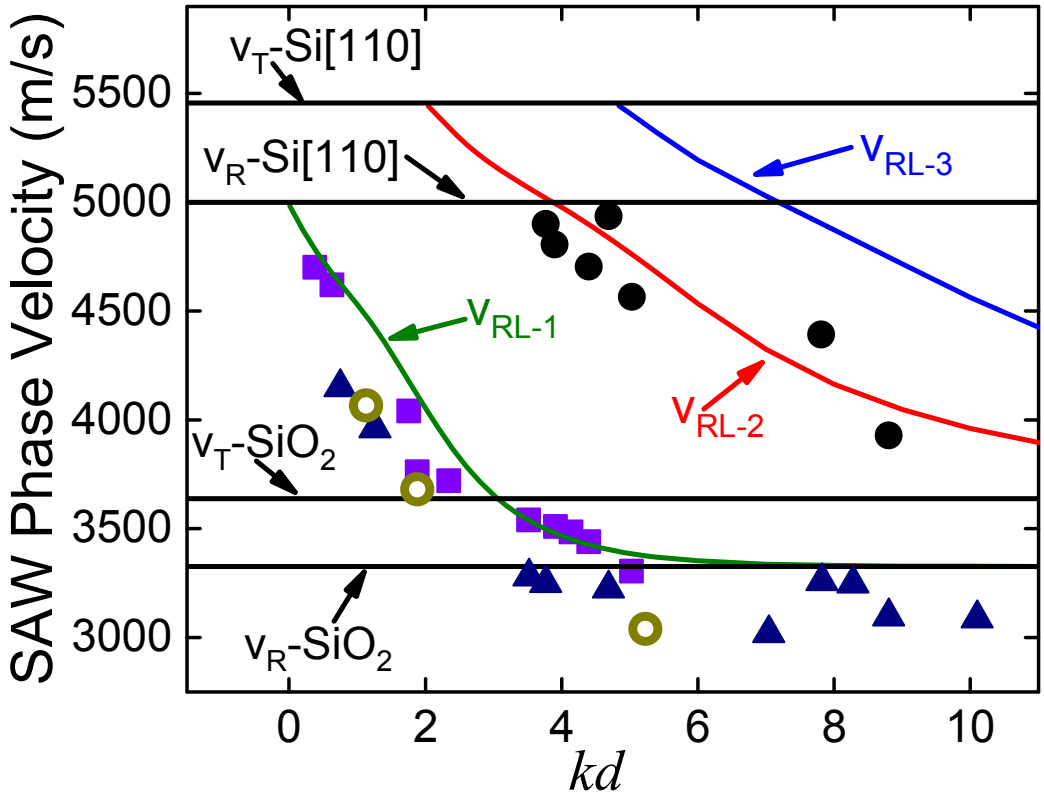

Figure 3: Phase velocity v of the lowest frequency mode detected on the ten samples (■) as determined by the formula $v = f\lambda$ where λ = pitch p. The calculated phase velocity for the first three Rayleigh-like surface wave modes for isotropic SiO_2 on Si are plotted with the green, red, and blue solid curves respectively. The (▲) and (○) symbols represent the measured frequencies that correspond to the RL-1 modes for the $\lambda = p/2$ and $p/3$ cases, respectively. The RL-2 (Sezawa) modes identified in the experiment and reported in Table II are plotted as well (●). The transverse velocity and Rayleigh wave velocity for Si [110] and SiO_2 are represented by the solid black lines.

Table I.

Sample (p/d in nm)	Freq. Meas. at 800 nm (GHz)	CGMD simulation (GHz)	IEC Calculation (no Al bars) (GHz)
1000/60	4.7	4.8	4.8
600/60	7.7	7.7	7.8
400/112	10.1	10.2	10.4
300/112	12.4	12.6	13.0
200/112	17.7	17.7	17.8
200/60	18.8	19.9	20.6
180/112	19.5	19.1	19.4
170/112	20.5	19.9	20.3
160/112	21.5	21.1	21.5
140/112	23.6	23.4	24.1

Table I: Column two contains the lowest measured frequency for the 10 samples in the study using the 800 nm probe configuration. Column three contains the CGMD simulated frequency of the RL-1 mode with $\lambda = p$ from column one. Column four contains the frequency of the RL-1 mode with $\lambda = p$ calculated using the methods of Ref. 8 for an isotropic elastic continuum (IEC) of SiO_2 on Si (with no Al bars).

surface. The simulation has no other source of damping, so unlike in the experiment, any pure surface mode that is excited will remain excited indefinitely. To simulate the pump-probe experiment, we heat the Al bars instantaneously in order to excite the possible modes of the structure. We then plot the Fourier transform of the displacement versus time over a range of a few thousand ps at various locations in the model. Once we have determined what the dominant frequencies are, we run the simulation a second time, this time driving the model at a particular frequency so that a visualization of each mode can be created. The simulations allow us to observe the perturbative effects of the presence of the 25 nm thick Al lines on the modes available to the structure. The frequencies of the lowest order Rayleigh-like mode provided by the simulation are given alongside the measured frequencies in column three of Table I and show a slightly improved agreement (maximum deviation of 5%) with the data as compared to the analytical calculation (column four). More importantly, the simulation allows us to visualize the modes to ensure that the motion is consistent with a Rayleigh-like SAW. Figures 4a and 4b are two frames of an RL-1 wave simulation for the p/d = 300nm/112nm sample driven at 12.6 GHz. The characteristic form of the RL-1 wave is that the displacement of the top and bottom of the SiO_2 layer are in phase with one another (the film is flexing). We have successfully modeled (with frequency matching to within 10% in all cases, better than 5% in most cases) nearly every one of the vibrational modes detected in the pump-probe experiment, including many of the higher frequency modes described in the following section. The simulations were executed with a precision of ± 0.2 GHz.

Higher frequencies

The pump-probe experiments have also shown a number of higher frequencies above the 1st order Rayleigh-like mode. This is in contrast to several similar experiments found in the literature, including our work of Ref. 6, but it is expected given the higher order modes illustrated by the solid curves of Fig. 3. In a 2009 paper, Maznev and Every calculated the Brillouin zone-folded SAW band structure for a sample whose structure is similar to the ones measured here. Their work showed that the presence of a periodic array of lines atop a film coated substrate produces hybridization of the first Rayleigh band with the Sezawa band, and that the expected frequencies are shifted from the case of a uniform film due to avoided crossings of these bands.[14] We also find a dependence on the wavelength of the probe light and the polarization of the probe light relative to the orientation of the lines.

Table II gives all of the frequencies measured on the 10 samples at the two probe wavelengths and for probe beam polarizations perpendicular (S-polarized) and parallel (P-polarized) to the orientation of the Al lines. The pump excitation of the nanostructure can excite SAWs with wavelength $\lambda = p, p/2, p/3 \ldots$. If the periodicity of the structure possessed a perfect 50% duty cycle we would not generate the even modes in this series, but we do observe the 2nd mode in every sample, even though the duty cycles as measured by SEM deviated from 50% by 10% or less. The measured frequencies that we associate with the $\lambda = p/2$ and $p/3$ RL-1 modes are

Figure 4

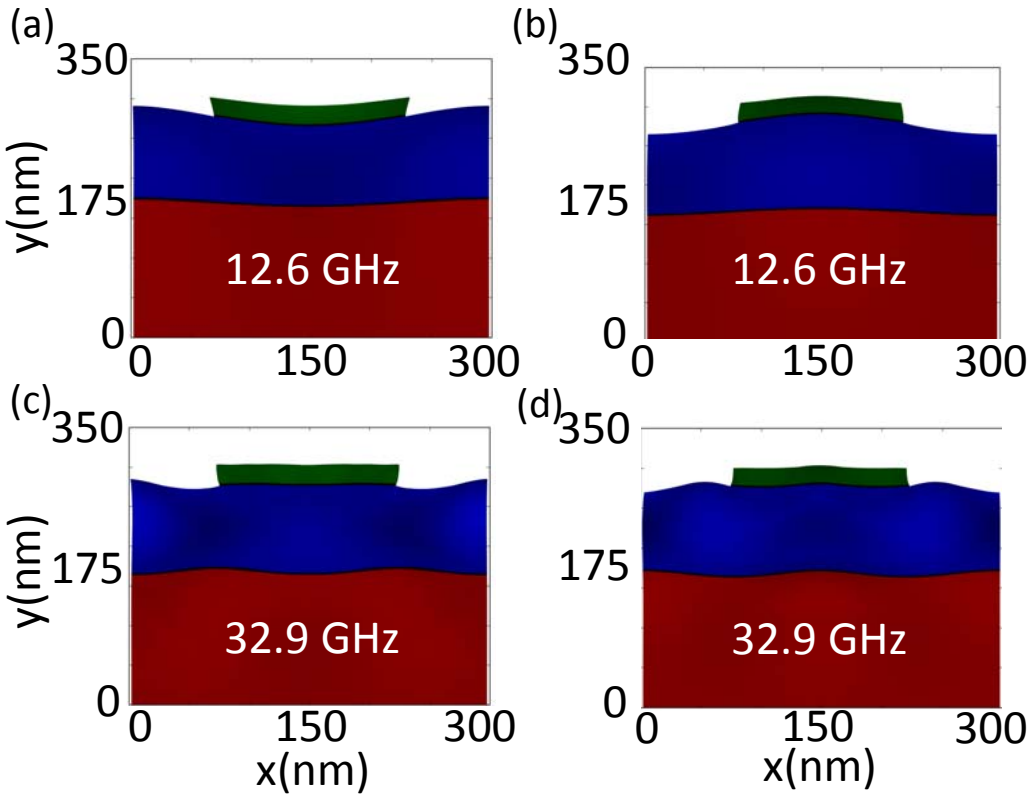

Figure 4: Coarse-grained molecular dynamics visualizations of two vibrational modes for the p/d = 300nm/112nm sample. Displacements are greatly exaggerated so that the character of the mode can be observed. (a) and (b) are two frames of the visualization for a 12.6 GHz RL-1 mode with λ = 300 nm that is detected in the experiment at 12.3-12.4 GHz. (c) and (d) are two frames of the visualization for a 32.9 GHz RL-2 mode with λ = 150 nm that is detected in the experiment at 32.9 GHz.

plotted alongside the lowest frequency modes in Fig. 3. Within experimental uncertainty, several of these modes have a measurably lower frequency and phase velocity than is predicted by the isotropic elastic continuum calculation - as much as 15% lower. Frequency shifts in the Rayliegh-like wave frequency away from the pure Rayleigh wave frequency are well known for periodic arrays of lines,[4,5,15] and the magnitude of the effect can be calculated by perturbation theory and is proportional to the ratio of the line thickness to the pitch, which is 25nm/p in our case. Since our data do not clearly demonstrate the pitch dependence of this effect, nor demonstrate the effect at all for the lowest frequency RL-1 modes, this remains for us a topic of a future study.

In addition to RL-1 modes, Table II also includes the RL-2 modes (also plotted in Fig. 3) and a few individual bar modes which is indicative that some of our data sets are very rich in frequencies. Fig. 5 shows the reflectivity data for 400 nm probe on the p/d = 200 nm/60 nm sample and its Fourier transform. When the probe light is P-polarized, only a single frequency is readily visible in the data, but when the probe light is S-polarized, seven frequencies are easily distinguished. The 18.8 GHz peak (which is relatively weak for S-polarized probe) is readily identifiable as the lowest frequency RL-1 wave, similar in shape to Figs. 4a and 4b. The strongest peak at 32.5 GHz differs only slightly from a small peak in the simulation at 35.3 GHz which corresponds to the $\lambda = p/2$ =100 nm RL-1 mode. The 29.9 and 48.8 GHz peaks compare well with a pair of modes from the simulation at 30.7 and 51.2 GHz which are RL-2 (Sezawa-like) modes with $\lambda = p$ = 200 nm and $\lambda = p/2$ = 100 nm respectively. The RL-2 modes have a characteristic breathing motion of the film like the simulation plotted in Figs. 4c and 4d. The phase velocity of the first of these two modes is higher even than the shear velocity in Si, and is predicted by the simulations to be a very short-lived mode. The 26.4 and 55.4 GHz modes are comparable to two modes from the simulation (27.8 and 55.4 GHz) that we have identified as individual modes of the Al lines themselves as opposed to a collective motion of the whole structure. Previous studies of this sort have also measured independent bar modes alongside SAWs,[1,2] and we discuss these modes later in this section. The remaining mode identified in Fig. 5 at 41.8 GHz (marked U in Table II for 'unidentified') is weakly predicted in the CGMD simulations at 42.6 GHz and is possibly caused by the longitudinal head wave propagating near the surface in the Si. A signal due to just such a wave was detected in the experiment of Miao et. al. in which a transparent mask was brought very near to a substrate and an ultrafast pump-probe scheme was implemented.[16] The signal would be expected at a frequency $f = v_{L,Si[110]}/p$ which is 45.5 GHz.

Comparison of the measured frequencies of Table II with simulated frequencies using the CGMD model allows us to label each reported frequency with a particular surface mode type from the simulation. The superscripts and subscripts identifying each SAW frequency's wavelength and mode type are explained in the caption of Table II. While RL-2 (Sezawa) waves (superscript b in Table II) in this frequency range have previously been observed by Brillouin

Figure 5

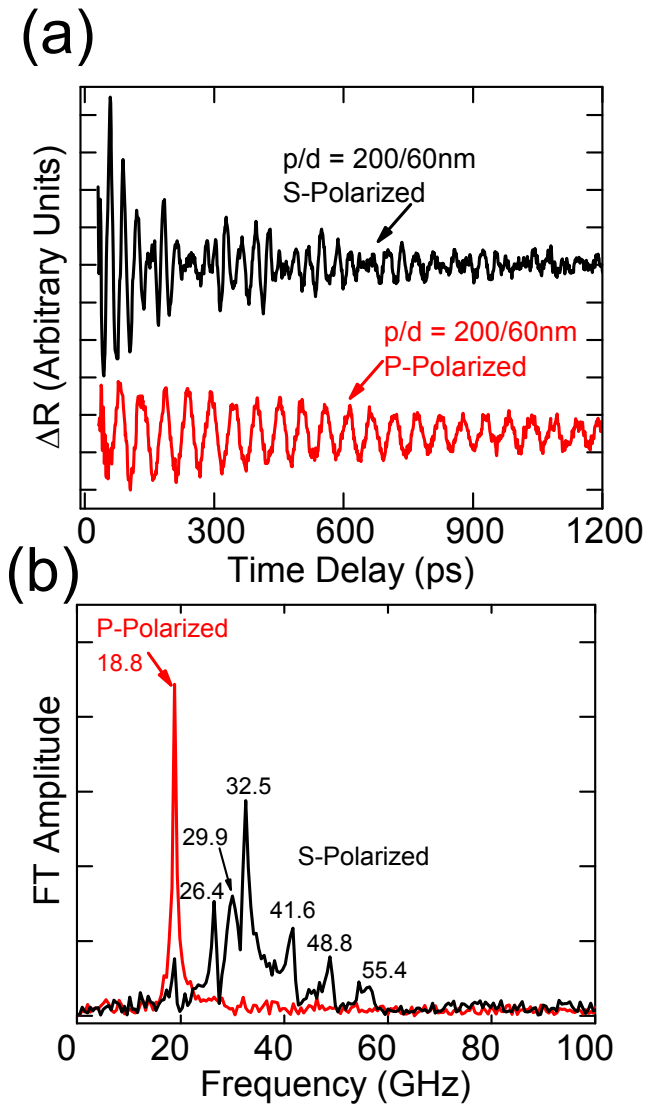

Figure 5: (a) ΔR for the p/d = 200 nm/60 nm sample using 400 nm probe in the S-Polarized and P-polarized configurations. (b) Fourier transform amplitude of the signals in (a).

Table II.

Sample (*p*/*d* nm)	400 nm P-pol. (GHz)	400 nm S-pol. (GHz)	800 nm P-pol. (GHz)	800 nm S-pol. (GHz)
1000/60	4.5^{1a}, 8.6^{2a}	4.5^{1a}, 8.1^{2a}, 12.2^{3a}, 15.2^{4a}	4.7^{1a}, 8.2^{2a}, 12.3^{3a}	4.7^{1a}, 8.2^{2a}, 12.1^{3a}, 20.2^{4a}
600/60	7.6^{1a}	7.6^{1a}, 13.7^{2a}, 18.2^{3a}	7.7^{1a}, 12.7^{2a}, 18.4^{3a}, 27.8^{4a}	7.7^{1a}, 13.3^{2a}, 18.5^{3a}, 27.8^{4a}
400/112	9.8^{1a}, 16.4^{2a}	10.0^{1a}, 16.4^{2a}, 22.8^{3a}	10.1^{1a}, 16.4^{2a}	10.1^{1a}, 16.4^{2a}
300/112	12.3^{1a}, 21.1^{2a}	12.3^{1a}, 21.1^{2a}, 32.9^{2b}	12.4^{1a}, 21.7^{2a}	12.4^{1a}, 21.8^{2a}
200/112	17.7^{1a}	-, 30.0^{2a}	17.7^{1a}	17.1^{1a}, 30.4^{2a}
200/60	18.8^{1a}	18.8^{1a}, 26.4^{B}, 29.9^{1b}, 32.5^{2a}, 41.6^{U}, 48.8^{2b}, 55.4^{B}	18.8^{1a}	19.1^{1a}, 26.7^{B}, 30.5^{1b}, 32.5^{2a}, 44.9^{U}, 49.3^{2b}, 55.6^{B}
180/112	19.7^{1a}, -, 37.9^{2a}, 47.9^{2b}	-, -, 35.3^{2a}	19.5^{1a}, -, 36.1^{2a}, 49.5^{2b}	19.0^{1a}, 26.7^{1b}, 35.4^{2a}, 49.0^{2b}
170/112	20.8^{1a}, 38.0^{2a}	-, 38.0^{2a}	20.5^{1a}, 38.1^{2a}	19.8^{1a}, 38.7^{2a}
160/112	21.8^{1a}	-, -, 36.3^{B}, 39.4^{2a}	21.5^{1a}, -, 36.0^{B}, 37.7^{2a}, 49.1^{2b},	21.0^{1a}, 29.4^{1b}, 35.7^{B}, 38.9^{2a}, 48.4^{2b}
140/112	23.9^{1a}	-, -, 39.4^{B}	23.6^{1a}	24.1^{1a}, 32.6^{1b}, 38.9^{B}, 44.1^{2a}

Table II: All measured frequencies from the four configurations of the experiment. A "-" indicates that a lower frequency that was present in another configuration is missing from that configuration. Superscript key: 1: $\lambda = p$, 2: $\lambda = p/2$, 3: $\lambda = p/3$, 4: $\lambda = p/4$, a = RL-1 mode, b= RL-2 (Sezawa) mode, B = independent bar mode, U = unidentified mode

scattering,[17,18] the direct detection of coherent Sezawa waves above 10 GHz is not common. A 22.4 GHz signal from only one of the samples studied in Ref. 6 was found to agree with predictions from a highly simplified simulation of a Sezawa mode of that nanostructure. Previous studies using a transient grating technique more definitively detected Sezawa waves at frequencies close to 1 GHz.[19,20] As Table II indicates, however, in the present experiment we have identified at least one Sezawa mode on five of the ten samples. These modes range in frequency from 30 GHz to 48 GHz and are found to match the CGMD simulated frequencies to better than 10% in all cases. Figure 3 includes the eight detected RL-2 (Sezawa) modes alongside the phase velocity graph for that mode for the isotropic elastic calculation for SiO_2 on Si, and the trend is comparable.

The data on three of the samples (p/d = 200 nm/60 nm, 160 nm/112 nm, and 140 nm/112 nm) exhibit frequencies that do not correspond to surface wave-like motion, but rather to modes of an individual bar attached to an SiO_2/Si substrate. These frequencies are marked with the superscript *B* in Table II. In Ref.1, Lin et. al. determined that the vibrational frequencies of gold bars on SiO_2 that they detected were not collective oscillations of many bars, but were instead either flexural (F) or longitudinal (L) modes of individual free bars perturbed by contact with the substrate. Figure 6 of Ref.1 shows the displacement patterns of the F and L modes, and Fig. 7 of Ref. 1 shows how those mode frequencies vary as a function of the Young's modulus of the substrate. To justify our assertion that these particular frequencies correspond to these individual bar modes, we have run our CGMD simulation for an isolated bar in order to remove the possibility of confusion with the collective SAW modes. In Table III, we compare the simulated frequencies for the case of isolated and non-isolated bars and find excellent agreement between the two versions of the simulation for these modes. The fact that the measured frequencies are 15% larger than the simulated ones for the p/d = 160 nm/112 nm and 140 nm/112 nm samples may indicate a systematic error in the reported width of those bars.

While our ability to detect particular modes does seem to have a sample to sample variation that prevents us from making definitive statements about the conditions for mode detection, one obvious trend can be observed. For both wavelengths, the S-polarized probe is more sensitive to higher frequencies than the P-polarized probe. In fact, at 400 nm, there are five cases for which the S-polarized probe shows no (or barely distinguishable above the noise level) sensitivity to the RL-1 SAW with $\lambda = p$, in spite of sensitivity to one or more higher frequency modes and despite there being a strong signal with P-polarization. Figure 6 illustrates this effect for the p/d = 180 nm/112 nm sample; the P-polarized signal is dominated by the 19.7 GHz signal (due to an RL-1 SAW with λ = 180 nm), and is accompanied by 2 higher frequency modes, but the S-polarized exclusively carries the 35.3 GHz signal (due to an RL-1 SAW with λ = 90 nm).

Polarization effects in picosecond ultrasonic experiments on nanostructures have been discussed before, [3,13,21,22] but a thorough explanation remains absent from the literature. The ΔR signal

Table III.

Sample (p/d nm)	Al Bar Cross section (nm)	CGMD Sim Freq. (GHz)	CGMD Sim Freq. Isolated (GHz)	Meas. Freq at 400 nm probe (GHz)
200/60 F	100 × 25	27.8	26.9	26.4
200/60 L	100 × 25	55.2	54.9	55.4
160/112 F	80 × 25	32.4	31.9	36.3
140/112 F	70 × 25	36.2	35.9	39.4

Table III: Individual bar mode summary for the four modes labeled with the superscript B in Table II.

Figure 6

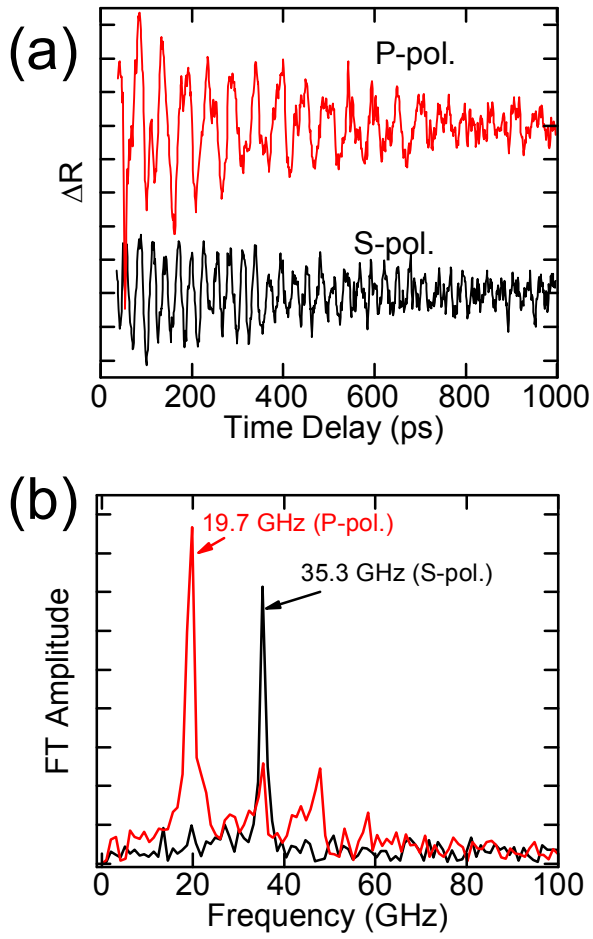

Figure 6: (a) ΔR for the p/d = 180 nm/112nm sample using 400 nm probe in the S-Polarized and P-polarized configurations. (b) Fourier transform amplitude of the signals in (a).

caused by the SAW should have two primary components – a piezo-optic component caused by strain induced changes in the optical constants of the Al lines, and a displacement component caused by the vertical and lateral movement of the lines themselves during the surface wave motion. The piezo-optic component is expected to be much stronger for an 800 nm probe rather than a 400 nm probe due to the d-band transition in Al near 1.5 eV[23,24] and this is the reason why the 800 nm data shows no missing low-frequencies in column 4 of Table II, unlike the 400 nm data in column 2.

The strong effect of probe polarization on the experiment is not surprising when we consider the shape of the electric and magnetic field functions in the near field of the optical grating presented by this relatively simple nanostructure. While an accurate prediction of ΔR as a function of the time-dependent strain caused by the SAWs is beyond the scope of this work, we have performed finite element calculations using COMSOL of the probe laser field amplitude for the samples in the experiment. Figure 7 shows the normalized field amplitude for S-polarized and P-polarized 400 nm light incident on the p/d = 180 nm/112 nm sample. In the P-polarized case, the field near the lines takes on a periodicity similar to that of the lines, while in the S-polarized case there are sharp peaks in the field amplitude near the edges of the Al lines. These differences in the field near the Al lines for the S and P cases when coupled with the oscillatory motion of the lines due to the presence of a SAW are expected to cause changes in our far field sensitivity to SAWs with differing wavelengths and displacement patterns. In certain cases, such as the one illustrated in Fig. 6, these differences appear to completely reduce or eliminate our far-field sensitivity to the lowest frequency SAW available to the structure.

Summary

In summary, we have used picosecond laser ultrasonics to generate and detect high frequency SAWs in the GHz range on a patterned layered nanostructure of Al/SiO_2/Si. We have detected Rayleigh-like and Sezawa-like modes with frequencies as high as 50 GHz, as well as a number of independent bar modes. We have compared our results to analytical calculations of an SiO_2/Si structure and to coarse-grained molecular dynamics simulations of the complete structure in order to accurately label the detected modes. We also found a strong dependence of the sensitivity to specific modes on the polarization of the probe light, especially when using a frequency-doubled probe at 400 nm.

Acknowledgements

The authors acknowledge the support of National Science Foundation award number DMR-1709521 "RUI: Acoustic Phonons in Nanostructures: Surface Waves, Thermal Transport, and Imaging." The sample fabrication was performed at the Cornell NanoScale Facility, a member of the National Nanotechnology Coordinated Infrastructure (NNCI), which is supported by the

National Science Foundation (Grant ECCS-1542081). We also acknowledge technical assistance from Mr. Sushant Mahat.

Figure 7

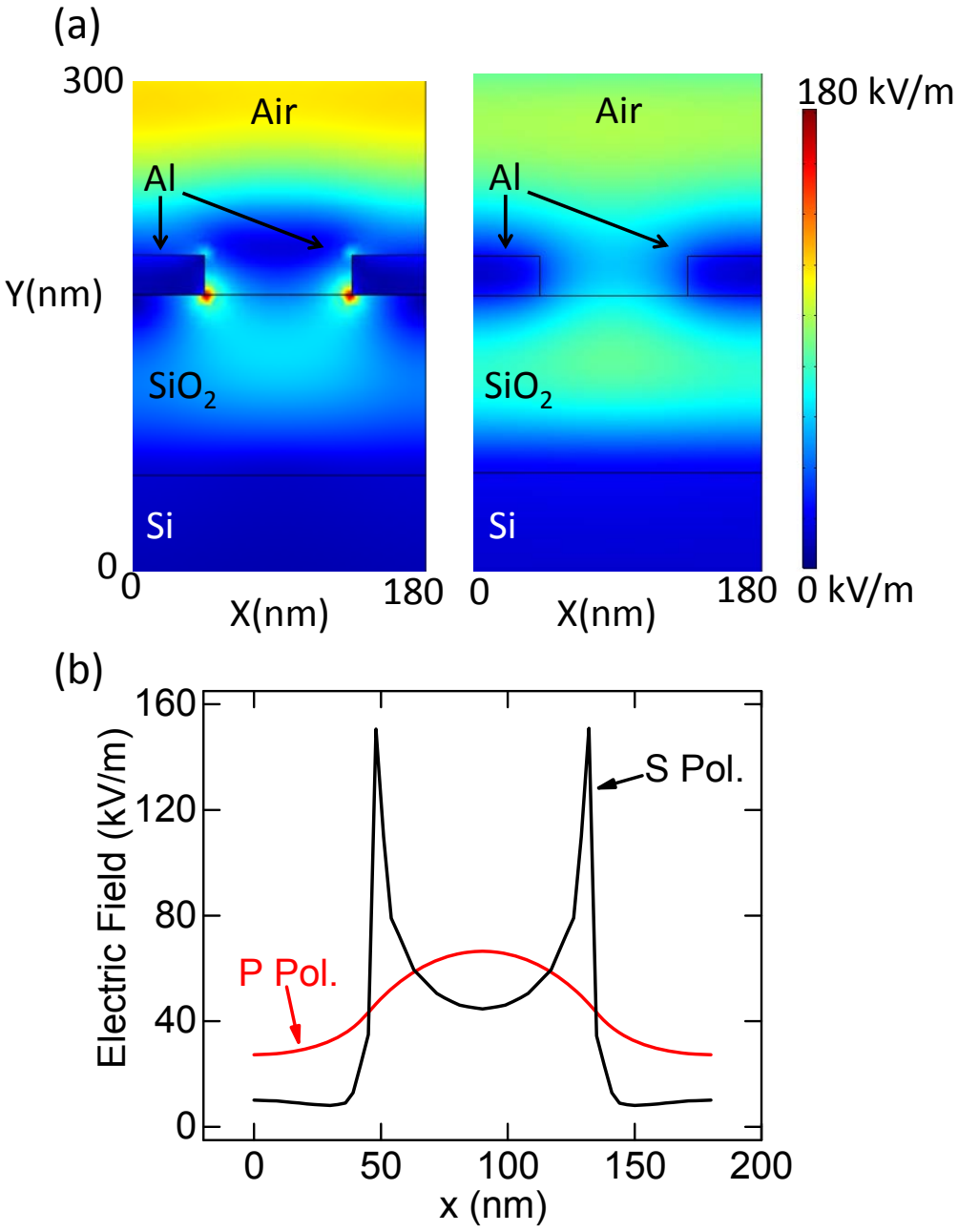

Figure 7: Finite element model of 400 nm probe light incident on p/d = 180 nm/112 nm sample. (a) Colormap of normalized electric field amplitude for S polarized (Left) and P polarized (Right) probe beam configuration. (b) Electric field amplitude as a function of lateral position taken at the Al pattern/SiO_2 interface for S and P polarizations.

[1]H.-N. Lin, H. J. Maris, L. B. Freund, K. Y. Lee, H. Luhn, and D. P. Kern, J. Appl. Phys. 73, 37 (1993).

[2] B. Bonello, A. Ajinou, V. Richard, P. Djemia, and S. M. Cherif, J. Acoust. Soc. Am. 110, 1943 (2001).

[3]D. H. Hurley and K. L. Telschow, Phys. Rev. B 66, 153301 (2002).

[4] J. Sadhu, J. H. Lee, and S. Sinha, Appl. Phys. Lett. 97, 133106 (2010).

[5] M. E. Siemens, Q. Li, M. M. Murnane, H. C. Kapteyn, R. Yang, E. H. Anderson, and K. A. Nelson, Appl. Phys. Lett. 94, 093103 (2009).

[6] M.M. Bjornsson et. al., J. Appl. Phys. 117, 095305 (2015).

[7] B. A. Auld, Acoustic Fields and Waves in Solids (Krieger Publishing Company, Malabar, Florida, 1990), Vol. 2, Ch. 10.

[8] G. W. Farnell and E. L. Adler, in Physical Acoustics, edited by W. P. Mason and R. N. Thurston (Academic Press, New York, 1972), Vol. 9, p. 35.

[9] G. A. Antonelli, B. Perrin, B. C. Daly, and D. G. Cahill, MRS Bull. 31, 607 (2006).

[10] C. Thomsen, H. T. Grahn, H. J. Maris, and J. Tauc, Phys. Rev. B 34, 4129 (1986).

[11] L.M. Brekovskikh, Sov. Phys. Acoust. 5, 288 (1960).

[12] D. Gelda, J. Sadhu, M.G. Ghossoub, E. Ertekin, and S. Sinha, J. Appl. Phys. 119, 164301 (2016).

[13]G. A. Antonelli, H. J. Maris, S. G. Malhotra, and J. M. E. Harper, J. Appl. Phys. 91, 3261 (2002).

[14] A. A. Maznev and A. G. Every, J. Appl. Phys. 106, 113531 (2009).

[15] H. Robinson, Y. Hahn, and J.N. Gau, J. Appl. Phys. 65, 4573 (1989).

[16] Q. Miao, L.-W. Liu, T.J. Grimsley, A.V. Nurmikko, and H.J. Maris, Ultrasonics 56, 141 (2015).

[17] N.L. Rowell and G.I. Stegeman, Phys. Rev. Lett. 41, 970 (1978).

[18] J.G. Dil, Rep. Prog. Phys. 45, 285 (1982).

[19] A. A. Maznev, Phys. Rev. B 78, 155323 (2008).

[20] A. A. Maznev and O. B. Wright, J. Appl. Phys. 105, 123530 (2009).

[21] D. Li, P. Zhao, J.-C. Zhao, and D. G. Cahill, J. Appl. Phys. 114, 143102 (2013).

[22] Q. Miao, L.-W. Liu, T.J. Grimsley, A.V. Nurmikko, and H.J. Maris, Ultrasonics 56, 141 (2015).

[23] A. Devos, Ultrasonics 56, 90 (2015).

[24] A. Devos and A. Le Louarn, Phys. Rev. B 68, 045405 (2003).